Astronomy
&
Astrophysics

Asteroseismology and evolutionary status of Procyon A

J. Provost[1], G. Berthomieu[1], M. Martić[2], and P. Morel[1]

[1] Département Cassiopée, UMR CNRS 6202, Observatoire de la Côte d'Azur, BP 4229, 06304 Nice Cedex 4, France
e-mail: `janine.provost@obs-nice.fr`
[2] Service d'Aéronomie du CNRS, BP 3, 91371 Verrières-le-Buisson Cedex, France

ABSTRACT

Models of Procyon A satisfying the actual observational constraints, particularly the asteroseismic ones, are discussed. The oscillations of these models were computed and analysed. We looked for seismic signatures of the evolutionary status of Procyon A. We show that the behavior of the small frequency spacings, particularly $\delta\nu_{01}$ allows us to distinguish between main sequence and post-main sequence models, all satisfying the observational constraints on mass, effective temperature, radius, and surface metallicity of Procyon A. We also introduce a new seismic evolution criterion, ε, based on the comparison of the low and high frequency parts of the power spectrum. The comparison of the seismic properties of the models with the available asteroseismic observations does not allow us to definitely decide on the stage of evolution of Procyon A. Much more accurate frequencies must be obtained especially in the low-frequency domain to distinguish between the models.

Key words. stars: oscillations – stars: evolution – stars: individual: Procyon A

1. Introduction

Many works have been devoted to the study of the structure and evolutionary status of Procyon A through computation of models satisfying the observational constraints for mass, effective temperature, metallicity, and, more recently, radius and asteroseismic frequencies (Guenther & Demarque 1993; Chaboyer et al. 1999; Kervella et al. 2004; Provost et al. 2004; Eggenberger et al. 2005; Straka et al. 2005).

Using seismic measurements in Eggenberger et al. (2004), Eggenberger et al. (2005) determine global constraints for the age, initial helium and metallicity contents, and for the mixing length parameter of Procyon A. They conclude in favor of a main sequence model with a mass of 1.497 $M_\odot$. Kervella et al. (2004) measured the diameter of Procyon A and discussed its evolutionary state, and conclude that Procyon A is ending its life on the main sequence. Preliminary results of Provost et al. (2004), considering only the frequency measurements of Martić et al. (2004) and models with a simplified equation of state, favored more evolved models.

In this paper, we try to determine how the age and structure of Procyon A can be derived from all the observational constraints. We do not search for the best model that fits the observations, but our aim is instead to delimit the range of models compatible with the observations within their uncertainties and some uncertainties of the physics and to point out the observational improvements that would allow us to select the best model. First we discuss the observational constraints (Sect. 2). Then, we proceed in two steps to determine how all these observations constrain our knowledge of the age, evolutionary status, and structure of Procyon A. In the first one, models with different masses, chemical compositions, and convection parameters, which together fulfill the constraints of Table 1, have been computed (Sects. 3 and 4). In a second step we study their asteroseismic properties and determine criteria that would help to distinguish between these models (Sect. 5). Finally we apply

Table 1. Adopted constraints for our models of Procyon A: mass $M_\star$, effective temperature $T_{\rm eff}$, radius $R_\star$, surface metallicity [Fe/H]$_{\rm s}$, and galactic enhancement $\Delta Y/\Delta Z$.

1.36	$< M_\star/M_\odot <$	1.48	AP02 + Hipparcos
6480	$< T_{\rm eff} <$	6580	AP02
2.023	$< R_\star/R_\odot <$	2.073	Kervella et al. (2004)
–0.08	$<$ [Fe/H]$_{\rm s} <$	–0.02	AP02
1.5	$< \Delta Y/\Delta Z <$	4.	

these criteria to the observed frequencies (Sect. 6) and conclude (Sect. 7).

2. Observational constraints

Different estimates of the mass of Procyon A have been made by measuring the orbit of the astrometric binary system Procyon A and B. The estimate of the masses depends on the value of the parallax used. With the parallax and astrometric data from HST-WFPC2 observations (Girard et al. 2000), Allende Prieto et al. (2002) (hereafter referred to as AP02) estimated the mass of Procyon A in the range between 1.41 $M_\odot$ and 1.53 $M_\odot$. Adopting the very precisely measured parallax by Hipparcos, the same authors derived a lower mass range (see Table 1) that we used to constrain our models. This is in agreement with the recent astrometric study of Procyon by Gatewood & Han (2000), who give a mass of 1.43 ± 0.034 $M_\odot$ for Procyon A.

The effective temperature of Procyon A is taken from AP02. Kervella et al. (2004) measured the angular diameter of Procyon A with VINCI/VLTI instrument and, using Hipparcos parallax, derived a linear diameter of 2.048 ± 0.025 relative to the solar diameter. The constraints on effective temperature and radius induce two limit values for the luminosity, namely $0.811 < \log(L_\star/L_\odot) < 0.859$. This range is included in the range
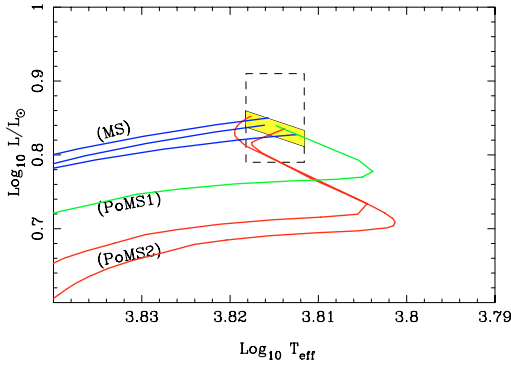
Fig. 1. Examples of main sequence (MS) and post-main sequence (PoMS1 and PoMS2 – see description in text) models satisfying the observational constraints for Procyon A: its position in the HR diagram constrained by effective temperature and the luminosity from Steffen (1985) (dashed box); the VINCI/VLTI (Kervella et al. 2002) radius measurement reduces the possible domain (grey area).

given by Steffen (1985). All these constraints define an area in the HR diagram where the models must be located (see Fig. 1).

The surface metallicity of Procyon A has been estimated by AP02. The constraint on surface metallicity is related to the solar metallicity by $[Fe/H]_s \sim \log(Z/X)_s - \log(Z/X)_\odot$ (Morel et al. 2000), where Z and X are the mass fraction of heavy elements and hydrogen. We used the standard solar metallicity of $(Z/X)_\odot = 0.0245$.

In order to satisfy the constraint from the chemical evolution of the galaxies, the initial values of $(Z/X)_i$ and Y_i were chosen according to Chaboyer et al. (1999) such that $1.5 < \Delta Y/\Delta Z < 4$ with primordial helium equal to 0.24 (see Fig. 4).

A constraint on the age can be deduced from the binarity of Procyon A. Provencal et al. (2002) discuss the cooling time of the white dwarf Procyon B and find that the progenitor ended its lifetime 1.7 ± 0.1 Gyr ago. If the mass of the progenitor is around 2.5–3 $M_\odot$ and has a solar metallicity, its lifetime on the main sequence (MS) is around 600–400 Myr. This lifetime is slightly shorter if the progenitor has a sub-solar metallicity (Bressan et al. 1993). This would lead to an age of Procyon A on the order of or larger than 2000 Myr.

Recently, Martić et al. (2004) and Eggenberger et al. (2004) identified peaks of frequencies of acoustic modes with degrees $\ell = 0, 1, 2$ in the power spectrum of Doppler-shift measurements. This corresponds to acoustic waves stochastically excited by the convective envelope with frequencies obeying quasi-asymptotic relations. As in the solar case (Gough 1991), the set of frequencies is characterized by the large and small frequency spacings defined by:

$$\Delta\nu_{n,\ell} = \nu_{n,\ell} - \nu_{n-1,\ell} \tag{1}$$

$$\delta\nu_{02} = \nu_{n+1,\ell=0} - \nu_{n,\ell=2} \tag{2}$$

$$\delta\nu_{01} = 2\nu_{n,\ell=0} - (\nu_{n,\ell=1} + \nu_{n-1,\ell=1}). \tag{3}$$

where n is the radial order of the oscillation.

In the high-frequency range, the large frequency spacing $\Delta\nu_{n,\ell}$ does not vary much with the frequency and is somewhat independent of the degree of the oscillation modes.

An estimate of the mean of the large frequency spacings $\overline{\Delta\nu}_{obs}$ in the observed spectrum of Procyon A as made by Martić et al. (2004) using the so-called "comb response method" gives $\overline{\Delta\nu}_{obs} \sim 53.5 \pm 0.5$ μHz in the frequency range of
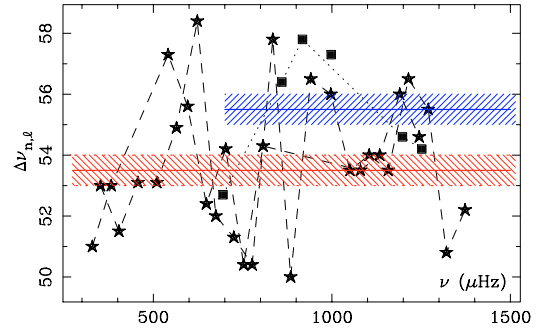

Fig. 2. Large frequency spacings $\Delta\nu_{n,\ell}$ for degrees $\ell = 0$ and $\ell = 1$ for frequencies of Martić et al. (2004) (star) and Eggenberger et al. (2004)(square). The hatched areas indicate the values of mean large frequency spacing $\overline{\Delta\nu}_{obs}$ for the two sets of observations (lower for the Martić's data).

the excess power between 300 to 1400 μHz. If the frequency range is restricted to the high-frequency part, $\overline{\Delta\nu}_{obs}$ is higher, around 54.5 μHz. For about the same high-frequency range, Eggenberger et al. (2004) estimate this mean value by adjusting an echelle diagram to the different peaks of the observed spectrum and obtain a higher value $\overline{\Delta\nu}_{obs} \sim 55.5 \pm 0.5$ μHz (Fig. 2).

Eggenberger et al. (2004) mention an error of 0.57 μHz for frequency determination, corresponding to half of the time resolution, but they notice that the dispersion of the observed large frequency spacings around the theoretical curve is higher. The difference between the estimations of $\overline{\Delta\nu}$ is larger than the errors given by the observers. The mean spacing is essentially proportional to the characteristic frequency $\sqrt{GM_\star/R_\star^3}$ (where $M_\star$ and $R_\star$ are the mass and the radius of the star). A difference in the quantity $\overline{\Delta\nu}$ in the high-frequency range of 1 μHz leads to a difference in mass at a constant radius of 3.6% and a difference in radius at a constant mass of 1.2%, which is on the order of the uncertainty of the observational determination of the mass and the radius of Procyon A. According to the adopted value of $\overline{\Delta\nu}_{obs}$, it is expected that different models of Procyon A will be selected. Recently MOST data on Procyon were obtained (Mathews et al. 2004). These data are contaminated by scattered Earthlight, modulated by the 101.413 min orbital period of the satellite, and their analysis is controversial. However, some estimation of $\overline{\Delta\nu}_{obs}$, about 54.5 μHz, is given by Regulo & Roca-Cortes (2005) and Garcia et al. (2006).

The observed small frequency spacings $\delta\nu_{02}$ and $\delta\nu_{01}$ are given in Fig. 3. Errors on the observed spacings are not provided by the authors. Identification of the successive modes is not always available due to aliases, destructive interferences with noise background, and the finite lifetime of modes. Martić & Lebrun (2006) use the technique of 2D collapsograms, which allows the exploration for the best signature of the mean spacings in different frequency regions of the excess power, independent of the mode degree. The significant departure of the modes in the region of the maximum oscillation amplitudes from the asymptotic relation explains the difficulties in finding the mean main frequency separation.

3. Procyon A modeling

All the models were computed with the CESAM code (Morel 1997), with the following physics: nuclear data from NACRE collaboration (Angulo et al. 1999), CEFF equation of state,
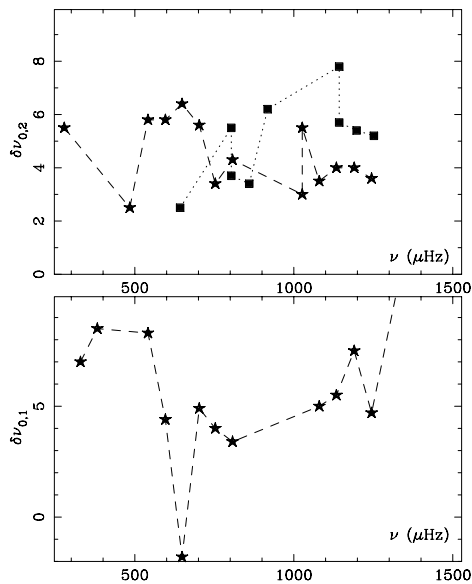
Fig. 3. Small frequency spacings $\delta\nu_{02}$ and $\delta\nu_{01}$ for the frequencies of Martić et al. (2004) and Eggenberger et al. (2004). The same symbols as in Fig. 2.

Fig. 4. Initial chemical composition of our models for Procyon A satisfying the constraints of Table 1. Grey open symbols indicate MS models, dark filled symbols PoMS models. Diamond 1.36 $M_\odot$, circle 1.38 $M_\odot$, triangle 1.42 $M_\odot$, stars 1.44 $M_\odot$, square 1.45 $M_\odot$, diamond 1.46 $M_\odot$, cross 1.48 $M_\odot$. The two full lines indicate the minimum and maximum values of Y_i resulting from the constraint of the galaxy chemical evolution given in Table 1. The dotted line corresponds to a stronger constraint $\Delta Y/\Delta Z \leq 3$.

4. Global properties of the models

With fixed values of mixing length and overshoot parameters, the models depend on the mass, the initial metallicity and helium contents, and the age, or respectively, $M_\star$, $(Z/X)_i$ Y_i and t. These unknowns are adjusted to fit the observational constraints ie. T_{eff}, $R_\star$, [Fe/H]$_s$. Models of mass between 1.36 to 1.48 $M_\odot$ were considered. For each mass, mixing length, overshoot and additional mixing parameters, different sets of $(Z/X)_i$ and Y_i give models that fit the observational constraints of Table 1. We found models, either in main sequence with a small convective core and mass from 1.42 to 1.48 $M_\odot$ or later, in post main sequence (PoMS) with mass from 1.36 to 1.45 $M_\odot$. In the following we differentiate two types of PoMS models: PoMS1 models in the phase of disappearance of convective core and of increasing effective temperature and more evolved PoMS2 models after the exhaustion of the central hydrogen (central hydrogen less than 0.001). The evolutionary tracks of some models are given in Fig. 1.

The MS models correspond to the higher masses. When the mass decreases, some core overshoot must be included in the modeling to obtain more luminous models with evolutionary tracks crossing the constrained area in the HR diagram. If we restrict the core overshoot parameter ($\zeta \leq 0.2$), the mass of MS models must be larger than 1.41 $M_\odot$. The uncertainty on the radius induces a crossing time of the allowed region in the HR diagram (Fig. 1) of about 80 Myr. As seen in Figs. 4 and 5, MS models have ages below 2000 Myr and high values of Y_i and $(Z/X)_i$ ($Y_i \geq 0.3$, $(Z/X)_i \geq 0.030$). We note that the range of $(Z/X)_i$ of our models is wide compared to the range of the surface metallicity $(Z/X)_s$. Indeed, $(Z/X)_s$ depends not only on $(Z/X)_i$ and Y_i, but also on the mass (and consequently on the age) and on the description of the diffusion. If we restrict it to MS or PoMS models, the range of $(Z/X)_i$ is about half, from 0.026 to 0.032 for PoMS models and from 0.30 to 0.038 for MS models. The range is slightly wider for MS models because it appears that their surface metallicity is more sensitive to the description of the diffusion. The constraint from the galactic chemical evolution strongly limits the number of MS models with lower masses as seen in Fig. 4.

The PoMS models can be obtained for mass smaller than 1.46. The uncertainty on the radius induces a smaller

OPAL opacities fitted at low temperature with Alexander & Ferguson tables, Eddington law for the atmosphere description (see Morel et al. 1994). We define the stellar radius of a model as the bolometric one. The convection is described either with the classical mixing length theory (hereafter MLT), with a mixing-length parameter λ of order 1.9 close to the solar value (Morel et al. 1999) or according to Canuto & Mazitelli (1991) (hereafter CM) with a mixing-length parameter λ of order 1. For some models, an overshooting of the convective core over a distance equal to $O_v = \zeta \min(H_p, r_c)$, is introduced, where H_p and r_c are the pressure height scale and the radius of the convective core. We vary the overshoot parameter ζ from 0 to 0.2. This value is recommended by Schaller et al. (1992) and confirmed by results obtained for the Hyades (Perryman et al. 1998), contrary to Straka et al. (2005), who give an upper limit on Procyon A's core overshoot extent of ζ about 0.4.

The microscopic diffusion of chemical species is taken into account according to Burgers (1969), using the resistance coefficients of Paquette et al. (1986). For stellar models with mass larger than 1.4 $M_\odot$, the use of microscopic diffusion alone produces an important depletion of helium and heavy elements and a concomitant enhancement of the hydrogen content at the surface. Different ways have been used to overcome this problem. Eggenberger et al. (2005) introduce some turbulence due to rotation. Di Mauro (2004) suppresses diffusion in the outer layers "to be sure that helium and heavy elements are not totally drained out of the envelope". Chaboyer et al. (1999) include a wind mass loss in the diffusion equations that reduces the diffusion in the outer layers of the star model. According to the prescription of Morel & Thévenin (2002), we introduce an additional mixing proportional to the radiative viscosity (e.g. Mihalas & Weibel-Mihalas 1984), parameterized by Re$_\nu$. The parameter Re$_\nu$ has been calibrated by Morel & Thévenin to 1 ± 0.5 by comparison of their models to stellar observations of the Hyades, but the physical meaning of this efficient source of mixing has been questioned by Alecian & Michaud (2005).
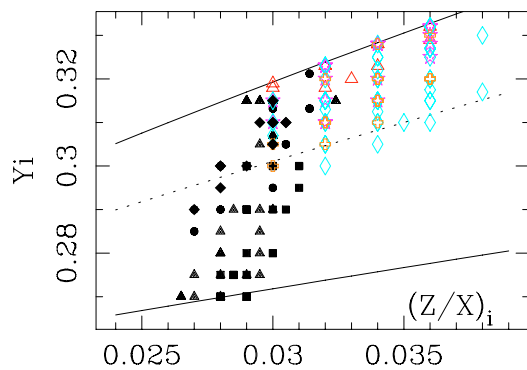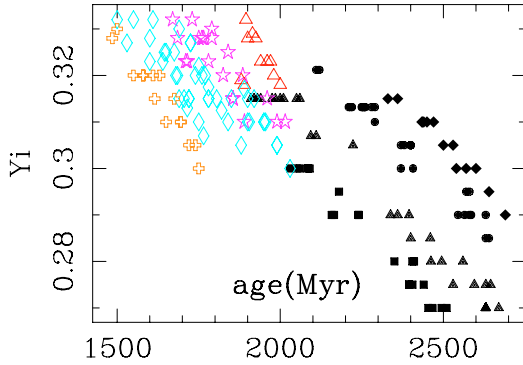
Fig. 5. Initial helium versus age. Same models and symbols as in Fig. 4.

Fig. 6. Frequencies $\nu_{G\ell}$ of the highest-frequency gravity modes for $\ell = 2$ and 3 versus the characteristic period P_0. The two regions where points are lacking correspond to the turning point of the evolutionary track in the HR diagram. There the models stay a very short time. Same models and symbols as in Fig. 4.

uncertainty on the age of less than 40 Myr. Within the range of MLT parameters we are considering, a majority of PoMS models do not have core overshoot. However, we find a few models with a very small core overshoot (ζ less or equal to 0.05). The PoMS models have lower values of Y_i and $(Z/X)_i$ than MS models and ages greater than 2000 Myr.

5. Asteroseismic properties of the models

Adiabatic frequencies of all the models were computed in the observed frequency range from 300 to 1500 μHz. We note that the upper limit is close to the acoustic cut-off frequency of the models.

The frequency of acoustic modes and the period of gravity modes can be respectively approximated by the following first-order asymptotic expressions:

$$\nu_{n,\ell} \sim \nu_0(n + \ell/2 + \vartheta_p) + O(1/\nu_{n,\ell}),$$

$$P_{n,\ell} \sim \frac{P_0}{\sqrt{\ell(\ell+1)}}(n + \vartheta_g) + O(1/P_{n,\ell})$$

with $\nu_0 = 2/\int_0^{R_\star} (dr/c)$ and $P_0 = 2\pi^2/\int_{RZ} (N/r)\,dr.$

Here c is the sound speed and N the Brunt-Väissälä frequency N ($N^2 = g(d\ln\rho/dr - 1/\Gamma_1 d\ln p/dr)$). The quantities ϑ_p and ϑ_g depend on the stellar atmosphere and on the stratification at the boundaries of the inner radiative zone (RZ), respectively, and they are of order unity. The quantity ν_0 is the inverse of the sound travel time across a stellar diameter. It varies very little for stars of given mass and radius and different chemical compositions. It is a theoretical estimate of the mean large spacing at high frequency.

5.1. Gravity and mixed-mode properties

The value of the characteristic period of gravity modes P_0 is given by the inverse of the integration of Brunt-Väissälä frequency in the inner radiative zone. The values of P_0 range from 10 to 50 min for PoMS models and from 50 to 80 min for MS models. For PoMS models P_0 corresponds to a frequency higher than ~800 μHz. This means that we may expect that the frequency domains of acoustic and gravity modes, which are well separated in solar type stars, are overlapping here.

For models in the early MS, the frequency range we consider corresponds to acoustic modes. Here the models are more evolved, and their spectrum contains some modes that are not
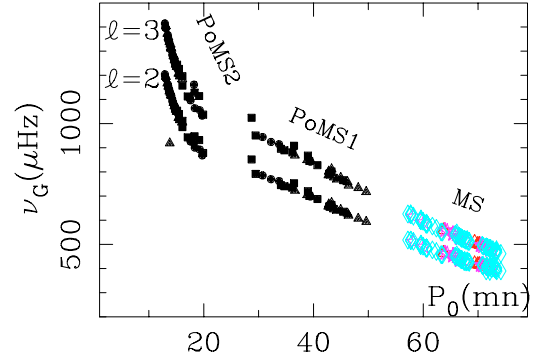
pure acoustic modes, but mixed and gravity modes. Indeed a large peak of the Brunt-Väissälä frequency, which may be as large as 1500 μHz, appears in the phase of central hydrogen burning due to the existence of a convective core and increases later on. This is seen in the propagation diagram (Fig. 7, left panel), where the local Brunt-Väissälä frequency, $N/2\pi$, and the local Lamb frequency, $S_\ell/2\pi$ ($S_\ell = \sqrt{\ell(\ell+1)}c/r$), are plotted as a function of the radius of the star. The gravity and acoustic modes are propagating in the regions of the star where their frequencies are smaller or larger than both N and S_ℓ, respectively. Thus gravity modes may exist with frequencies as high as the maximum of N. The frequency of the gravity modes of highest frequency, $\nu_{G2,3}$, are indicated for $\ell = 2$ and 3 by horizontal lines in the propagation diagram (Fig. 7, left panel). In contrast, for $\ell = 1$, we found no gravity modes in the considered frequency range, but only mixed modes.

The gravity modes are characterized by a large amplitude in the core of the star and consequently a much higher energy than the adjacent acoustic modes as seen Fig. 7 (right panel). In Fig. 8 the kinetic energy density is plotted for some modes: an acoustic mode, a gravity mode, and two mixed modes with both acoustic and gravity characters. If one assumes that all the modes in a given frequency range have the same total energy, the surface amplitude of gravity modes would be smaller than that of acoustic adjacent modes.

We studied the properties of the gravity modes with the highest frequency for $\ell = 2$ and 3. We find a strong correlation between their frequencies ν_G and the characteristic period of gravity modes P_0 (Fig. 6). Such modes are expected to have a small surface amplitude, but also very small line-width. They will be difficult to observe, but we hope that the new methods, which are being developed in the COROT frame for detecting such long-lived modes embedded in an acoustic spectrum (Moreira et al. 2005), may help to extract them from future observations. Knowing the frequency of these high-frequency gravity modes would give a new constraint on the evolutionary status of Procyon A.

5.2. Evolution criteria from the p-mode spectrum

Let us now consider the acoustic part of the spectrum. We define the following seismic quantity: $\overline{\Delta\nu}$, mean of the large frequency spacings $\Delta\nu_{n,\ell}$ computed with those frequencies higher than 800 μHz and with degrees $\ell = 0$ and 1. Most of our models
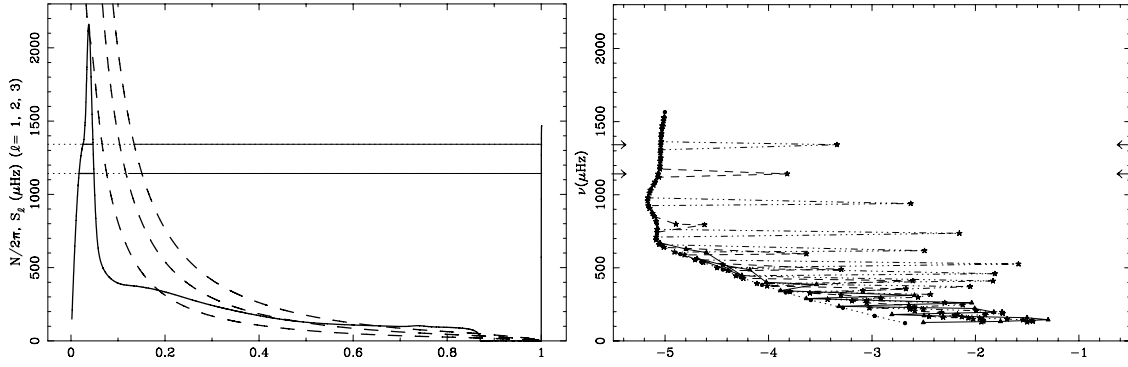
Fig. 7. *Left panel*: propagation diagram: variation of the Brunt-Väissälä frequency N (full line) and of the Lamb frequency S_ℓ ($\ell = 1, 2, 3$ dashed lines) in μHz as a function of the stellar normalized radius r for a PoMS model with mass 1.38 $M_\odot$. *Right panel*: frequency versus logarithm of the non-dimensioned kinetic energy E of the mode for consecutive modes of degree $\ell = 0$ (dotted), 1 (full), 2 (dashed), 3 (fancy) of the same model. The values of the highest frequency gravity modes for $\ell = 2$ and $\ell = 3$ are given by the horizontal lines in the left panel and by the arrows in the right panel. The heavy lines indicate the regions where these modes are propagative. Most of their amplitude is located in the core (see also Fig. 8 (1)).
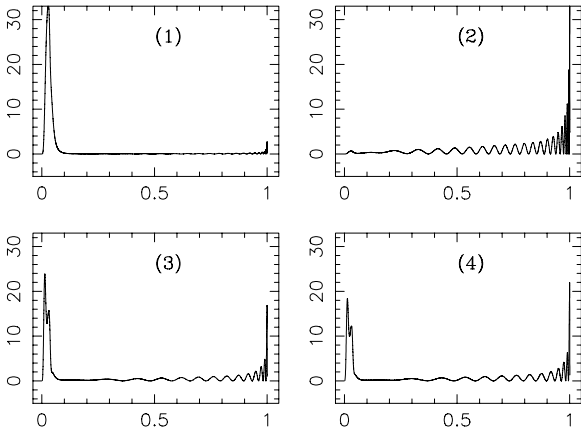

Fig. 8. Kinetic energy density as a function of the radius for different type of modes $\ell = 2$ of the same PoMS model as in Fig. 7: (1) gravity mode $\nu \sim 1144 \, \mu$Hz, (2) acoustic mode p20 $\nu \sim 1176 \, \mu$Hz, (3) and (4) two consecutive mixed modes $\nu \sim 994$ and $998 \, \mu$Hz in between the pure acoustic modes p12 and p14.

Fig. 9. Large frequency spacing normalized to the observed radius of Procyon A as a function of the mass. Its increase with respect to the mass is larger for PoMS than for MS models. Open (filled) symbols for MS (PoMS) models.

have a mean large frequency spacing $\overline{\Delta\nu}$ from 53.5 μHz to 57.5 μHz. However, the uncertainty on the radius induces an uncertainty on $\overline{\Delta\nu}$ of about 1 μHz. If we normalize this quantity to the radius of Procyon A given by Kervella et al. (2004), we obtain less dispersed values, which are plotted in Fig. 9 as a function of the mass. The remaining dispersion is due to the difference in chemical composition. At any given mass, the normalized large frequency spacing is larger for PoMS models than for MS models.

Figure 10 shows that the variations with the frequency in the large frequency spacings $\Delta\nu_{n,\ell}$ have a different behavior for degree $\ell = 0$ and 1 in the frequency range below 800 μHz. The few gravity modes $\ell = 2$ in the high-frequency range, which do not obey the asymptotic properties of p-modes, are not included in our computation of the frequency spacings.

For all the models, the curves representing $\Delta\nu_{n,\ell}$, for degree $\ell = 0$ are close within 3 μHz and compatible with the observations. They have a different behavior for degree $\ell = 1$ in the lower part of the frequency domain. Indeed contrary to the MS models, evolved models have many mixed modes in the low-frequency range, as seen in Fig. 7. This induces irregularities in the large frequency spacing for non radial modes. Thus
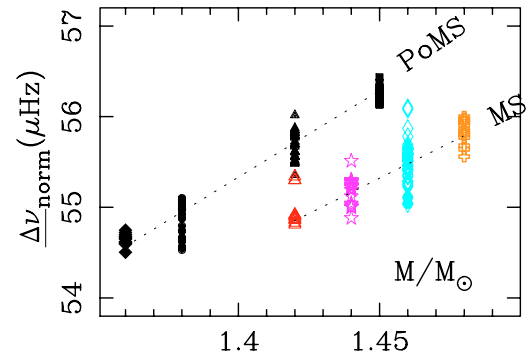
to measure the degree of evolution, we introduce the following quantity:

$$\varepsilon = (\overline{\Delta\nu} - \overline{\Delta\nu}_{\text{low}})/\overline{\Delta\nu}, \tag{4}$$

where $\overline{\Delta\nu}_{\text{low}}$ is the mean large frequency spacing at low frequency 500–800 μHz for $\ell = 1$. It is expected from Fig. 10 that ε will be very low for MS models and significantly high for PoMS models. Indeed this is seen clearly in Fig. 11, where ε is plotted as a function of $\overline{\Delta\nu}$. This shows that the determination of ε allows us to distinguish between MS and evolved models. If an observational determination of the mean large spacings can be obtained separately in the two frequency domains, $\overline{\Delta\nu}$ and $\overline{\Delta\nu}_{\text{low}}$, a difference between the two values higher than 3 μHz ($\varepsilon \geq 0.06$) would imply that the star is in the PoMS2 evolutionary stage.

The evolutionary stage of a star is strongly related to the structure of the stellar core, where the nuclear reactions modify the stellar stratification and density. The periods of the gravity modes are very dependent on the properties of this inner region. Figure 12 shows that there is a good correlation between ε and the quantity P_0.

Let us now examine the two small frequency spacings $\delta\nu_{02}$ and $\delta\nu_{01}$, which are combinations of acoustic modes penetrating differently towards the center and thus very sensitive to the central part of the stellar interior. For MS models, the variation
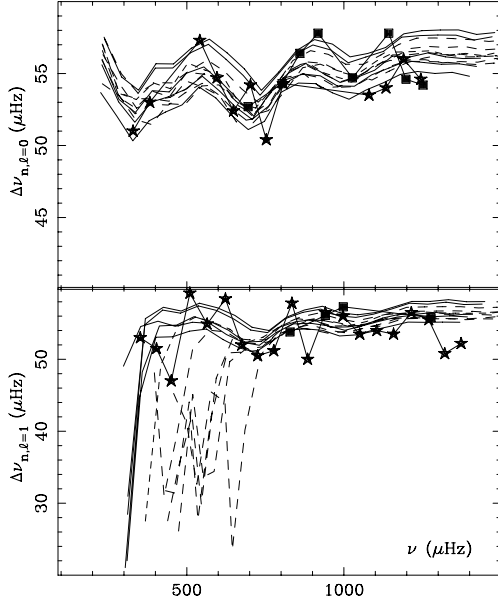
Fig. 10. Large frequency spacings for $\ell = 0$ (*up*) and 1 (*down*) for MS/PoMS models (full/dashed line) compared to Martić (stars) and Eggenberger (square) observations.
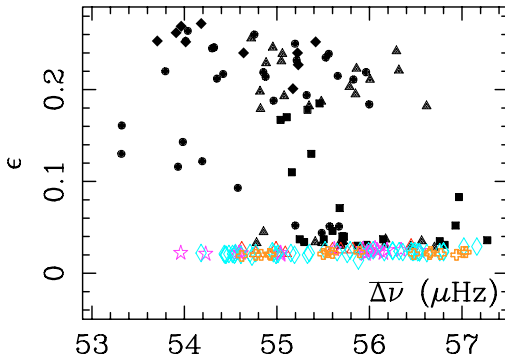

Fig. 11. Seismic quantity ε characterizing the model evolutionary stage versus the mean large frequency spacing $\overline{\Delta\nu}$. Grey open symbols indicate MS models, dark filled symbols PoMS models. Diamond 1.36 $M_\odot$, circle 1.38 $M_\odot$, triangle 1.42 $M_\odot$, stars 1.44 $M_\odot$, square 1.45 $M_\odot$, diamond 1.46 $M_\odot$, cross 1.48 $M_\odot$.

in $\delta\nu_{02}$ for radial order that is high enough can be roughly approximated as:

$$\delta\nu_{02} \approx \delta_0 + S_0(n - n_0). \qquad (5)$$

The variation in $\delta\nu_{01}$ is better approximated by a quadratic expression:

$$\delta\nu_{01} \approx \delta_1 + S_1(n - n_0) + \gamma_1(n - n_0)^2. \qquad (6)$$

Although the behavior of these small spacings is more complex for evolved models, we characterize the seismic properties of the models using the above global quantities δ_0, S_0, δ_1, S_1, and γ_1. The fit is made in the frequency range 800–1400 μHz, corresponding to a radial order from about 14 to 24 with $n_0 = 19$.

Figure 13 shows the slope S_0 and δ_0 that characterize the variation with the frequency of the small spacing $\delta\nu_{02}$. There, δ_0 is roughly the mean of $\delta\nu_{02}$ in the considered frequency range. For MS models, $\delta\nu_{02}$ decreases with the frequency and there is an almost linear relation between δ_0 and the negative slope S_0. The quantity δ_0 increases from 3.5 to 4.3 μHz for masses from 1.42 to 1.48 $M_\odot$.
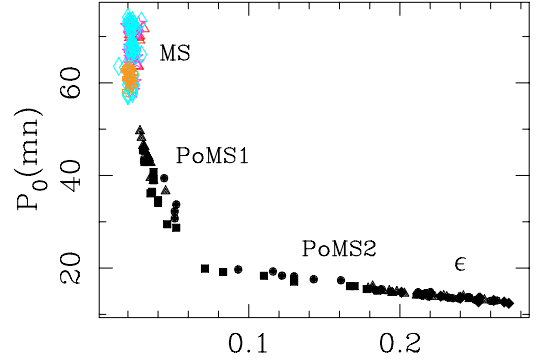

Fig. 12. Characteristic period P_0 of gravity modes as a function of the seismic quantity ε characterizing the model evolutionary stage.
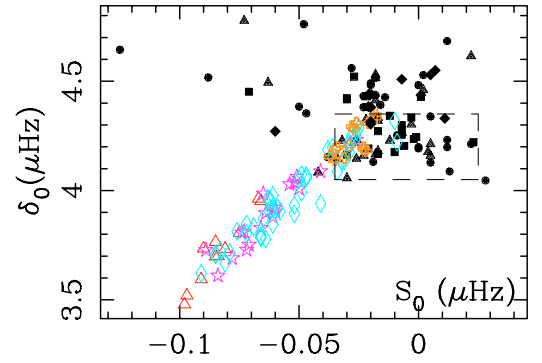

Fig. 13. Characteristics δ_0 and S_0 of the small frequency spacings $\delta\nu_{02}$. The dashed box indicates the location of PoMS1 models. Same models and symbols as in Fig. 11.
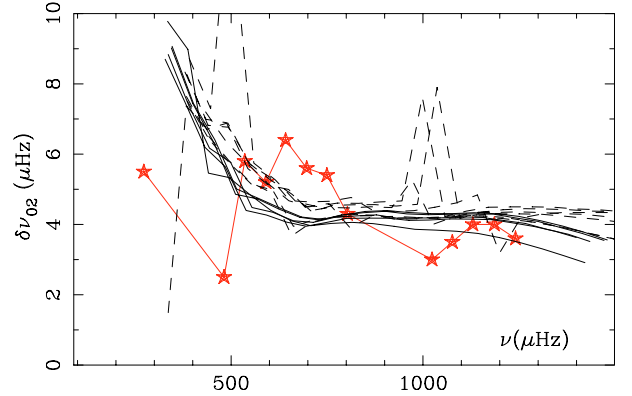

Fig. 14. Variation in the small frequency spacing $\delta\nu_{02}$ with the frequency for the same MS/PoMS models (full/dashed line) as in Fig. 10. The dashed line with the highest peak in the high-frequency range ($\nu \leq 800$ μHz) corresponds to the PoMS model with the lower negative value of the slope S_0 (model at the upper left corner in Fig. 13). If we perform a least-square linear fit removing the point at the peak, we obtain a slope $S_0 \sim -7 \times 10^{-4}$ μHz, instead of -0.125 μHz. This would move the corresponding point towards a region in continuity with MS models in Fig. 13.

For PoMS models the small spacing $\delta\nu_{02}$ has higher values, δ_0 higher than 4 μHz. The values of the slope S_0 are very dispersed, due to the fact that the quasi-linear variation of $\delta\nu_{02}$ with the radial order is perturbed around the frequencies of the mixed modes for $\ell = 2$. An example of this variation is given in Fig. 14, where a peak due to the presence of two consecutive mixed modes in $\ell = 2$ spectrum is clearly visible. Such peaks mainly influence the determination of the slope S_0 and explain
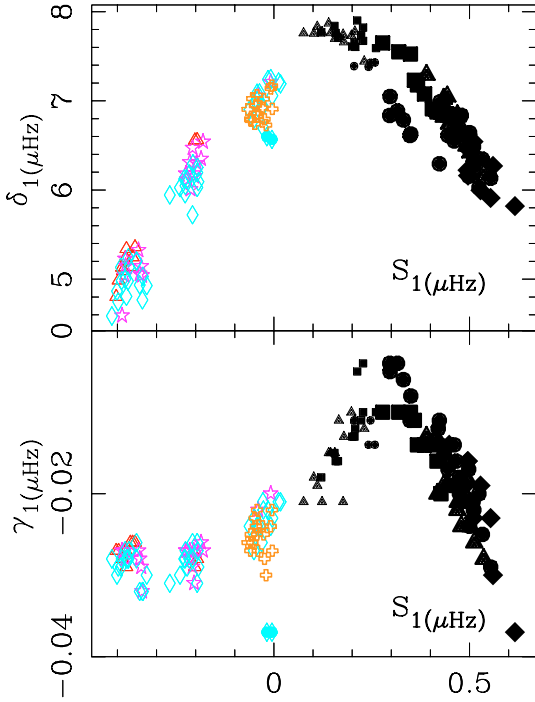
Fig. 15. Behavior of the small frequency spacing $\delta\nu_{01}$. Same symbols as in Fig. 13 (grey/dark for MS/PoMS models), but with different sizes for the PoMS models (dark symbols), the largest full symbols corresponding to the PoMS2 models (central hydrogen less than 0.001). *Upper panel*: δ_1 versus slope S_1. *Lower panel*: curvature γ_1 versus slope S_1. The three groups of points with $S_1 \leq 0$ correspond to models with different overshoot parameters, $\zeta = 0.2, 0.1$ and $0.$ from the left to the right.

the dispersion of the points corresponding to PoMS models in Fig. 13. However, the value of δ_0 can be used to distinguish between MS and PoMS models, except for the MS models of highest masses. This criteria is less selective in our case than in Straka et al. (2005).

Figure 15 shows the quantities δ_1, S_1, and γ_1 that characterize the variation with the frequency of the small spacing $\delta\nu_{01}$ (cf. Eq. (6)). For MS models, the small spacing $\delta\nu_{01}$ decreases with the frequency ($S_1 \leq 0$). The three groups of points with $S_1 \leq 0$ correspond to models with different overshoot parameters, $\zeta = 0.2, 0.1$ and 0.0 from the left to the right. The smallest values of δ_1 and S_1 correspond to the larger ζ value ($\delta_1 = 5 \pm 0.5\ \mu$Hz for $\zeta = 0.2$, $\delta_1 = 6.2 \pm 0.5\ \mu$Hz for $\zeta = 0.1$, $\delta_1 = 7 \pm 0.5\ \mu$Hz for $\zeta = 0$).

In contrast, the small spacing $\delta\nu_{01}$ increases with the frequency ($S_1 \geq 0$) for PoMS models. The values of δ_1 range from 6 to 8 μHz. Figure 15 shows that the highest values of $\delta\nu_{01}$ or δ_1 occur for the PoMS1 models. They have also the lowest positive values of S_1. The lower panel exhibits a negative "curvature" γ_1 for all the models of Fig. 15.

In conclusion, determining the sign of S_1 is a very good way to distinguish between MS and PoMS models. For MS models, its value indicates the amount of convective core overshoot in the core. In contrast, the quantity δ_1, which is close to a mean value of $\delta\nu_{01}$, cannot be used to characterize the evolutionary stage of a star such as Procyon A.

6. Discussion

In this section we present our results on Procyon A and compare them to previous works. We first consider the effects of the uncertainties on the global constraints in the modeling and evolution of Procyon A, and we discuss the sensitivity of our results upon the various assumptions about the physics used in this modeling (Sect. 6.1). Second, we try to derive information on the evolutionary status of Procyon A from the available seismic observations (Sect. 6.2).

6.1. Sensitivity to global constraints and physics

The observations of Procyon A give constraints on the mass, the effective temperature, the stellar radius and the surface chemical composition. Our results have shown that they are compatible with both MS and PoMS models. The MS models of Procyon A have high initial helium and heavy element contents. Their ages range from about 1400 to 2000 Myr. Their masses range from 1.42 $M_\odot$ to 1.48 $M_\odot$. For the lowest masses, some core overshoot is needed to satisfy the observational constraints. The PoMS models have lower masses, initial Y_i and $(Z/X)_i$ and larger ages. Note that due to the properties of its white dwarf companion, it is expected that Procyon A has an age of at least 2000 Myr (Kervella et al. 2004; Provost et al. 2004).

We used a high limit for the constraint linked to the chemical evolution of the galaxies $\Delta Y/\Delta Z$, as in Chaboyer et al. (1999). If we take a lower maximum value of this constraint, i.e. 3 instead of 4., most of the MS models would be ruled out, unless we accept higher mass and final surface metallicity. We have shown (Provost et al. 2005) that if microscopic diffusion of chemical species is not taken into account, the models satisfying the same constraints have lower initial helium content, thus lower $\Delta Y/\Delta Z$. This may explain why the models of Straka et al. (2005), which have higher surface metallicity and no envelope element diffusion, are mostly MS models.

We looked at the influence of the additional mixing parameter Re$_\nu$ related to radiative viscosity and of the descriptions of the convection on both the global and asteroseismic properties of the models.

Both MS and PoMS models satisfying the observational constraints for Procyon A and with given mass, age, and initial chemical composition have been computed for different values of the additional mixing parameter Re$_\nu$ from 0.5 to 1.5. Their properties are given in Table 2, and their evolutionary tracks and surface metallicity as a function of the age are given in Fig. 16. These different treatments of mixing do not modify the structure of the models much, which have same limit for the convection zone and convective core (for MS models), and thus their seismic properties. The surface metallicity is strongly modified relative to the uncertainty on the observed metallicity for MS models, which means that it depends strongly on the way diffusion is treated in the modeling. As seen in Fig. 16, the situation is very different for PoMS models, which are older at the end of hydrogen burning. Their surface chemical composition is almost insensitive to the value of Re$_\nu$. These results agree with the discussion by Provost et al. (2005), who studied the effect of varying the parameter Re$_\nu$ on the stellar modeling and frequencies.

We also considered models with different treatments of the convection and with different values of the mixing length parameter λ. Their properties are given in Table 3. Models with CM with $\lambda = 1$ and MLT with $\lambda = 1.7$ are very close. One important effect of varying λ concerns the surface metallicity of the model. For both MS and PoMS models with MLT, $(Z/X)_s$

Table 2. Global parameters of models differing by the way diffusion is treated varying the additional mixing parameter: (a) MS model of mass $M = 1.46\ M_\odot$, (b) PoMS model of mass $M = 1.38\ M_\odot$.

Re_ν	0.5	1	1.5
(a)			
t (Myr)	1600	1600	1600
$R_\star/R_\odot$	2.051	2.048	2.036
$(Z/X)_s$	0.0134	0.0180	0.0206
$[Fe/H]_s$	–0.263	–0.134	–0.075
Y_s	0.144	0.183	0.205
Xc	0.293	0.294	0.294
$r_{core}/R_\star$	0.078	0.078	0.078
$r_{env}/R_\star$	0.920	0.920	0.920
(b)			
t (Myr)	2400	2400	2400
$R_\star/R_\odot$	2.05	2.066	2.05
$(Z/X)_s$	0.0229	0.0228	0.0234
$[Fe/H]_s$	–0.029	–0.032	–0.020
Y_s	0.240	0.239	0.245
$r_{env}/R_\star$	0.870	0.870	0.871

Table 3. Global parameters of models differing by the way convection is treated: the Canuto & Mazitelli theory and $\lambda = 1.$, and the classical mixing length theory with $\lambda = 1.9, 1.7$. (a) MS models $M_\star = 1.46\ M_\odot$, (b) PoMS models $M_\star = 1.38\ M_\odot$).

λ	1.(CM)	1.9	1.7
(a)			
t(Myr)	1600	1690	1600
$R_\star/R_\odot$	2.048	2.049	2.043
$(Z/X)_s$	0.018	0.021	0.018
$[Fe/H]_s$	–0.134	–0.062	–0.129
Y_s	0.183	0.209	0.185
Xc	0.294	0.265	0.293
$r_{core}/R_\star$	0.078	0.076	0.078
$r_{env}/R_\star$	0.919	0.888	0.918
(b)			
t (Myr)	2255	2290	2260
$R_\star/R_\odot$	2.050	2.062	2.068
$(Z/X)_s$	0.0215	0.023	0.021
$[Fe/H]_s$	–0.057	–0.026	–0.068
Y_s	0.183	0.244	0.226
$r_{env}/R_\star$	0.904	0.880	0.905

well beyond the observational constraints. This result may come from the difference between the stellar evolutionary codes that are used. The model comparison, carried on in the COROT context (Monteiro et al. 2005), shows that the luminosity of models computed with the evolutionary code GENEC is systematically smaller than the luminosity obtained with our code.

6.2. Asteroseismic criteria and observations

All the models of Procyon A that we computed satisfying the observational constraints of Table 1 have mean large frequency spacing from 53 to 56.5 μHz, compatible with the range of values given by different observers. Our results show that a low value of the mean large frequency spacing $\overline{\Delta\nu}$ would favor PoMS and MS models of low mass. However, we must keep in mind that low-mass MS models need to be initialized with a large $\Delta Y/\Delta Z$ close to the upper limit (close to 4) given by the galactic chemical evolution.

We have derived several criteria to establish the evolutionary stage of Procyon A. First, looking in the low frequency range where mixed modes appear when the star is evolved, we introduced a parameter ε that characterizes the behavior of the $\ell = 1$ large frequency spacing. It allows us to distinguish between the models, as it is very small for MS models and increases up to 0.25 for PoMS models. If we compute ε for the available observations (Martić et al. 2004), we obtain a low value $\varepsilon \sim 0.018$. If we assume that mixed modes have enough energy to be observed, such a low value of ε would indicate that Procyon A is in MS phase.

In the high-frequency range, the mean small spacing $\delta\nu_{02}$ gives a way to establish the stellar evolutionary stage as in Straka et al. (2005), but in our case the separation of the two groups of models is not as sharp. This may be due to the choice of the frequency domain on which the mean δ_0 is estimated. Straka et al. (2005) consider larger radial orders corresponding to higher frequencies. For PoMS models, the slope of $\delta\nu_{02}$ as a function of the frequency is small, and the mean of $\delta\nu_{02}$ is not sensitive to the frequency domain. In contrast, for MS models the decrease in $\delta\nu_{02}$ with the frequency is noticeable (Fig. 13), and its mean value decreases if we take a higher-frequency range, leading to a better separation between PoMS and MS models. If we consider the observations of Eggenberger et al. (2004), we obtain
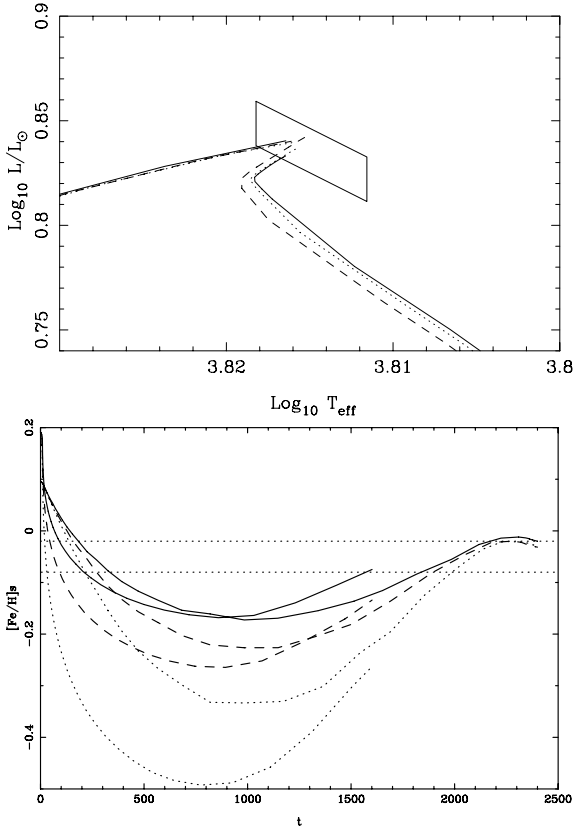

Fig. 16. MS and PoMS models computed with different values of the additional mixing parameter (cf. Table 2): $Re_\nu = 0.5$ (dotted line), 1. (dashed line), 1.5 (full line). The evolutionary tracks and final position in the HR diagram are very close (*higher panel*). The variation in surface metallicity as a function of the age and its final value are very different for MS models (*lower panel*).

increases when the value of λ increases. As expected, when λ increases by 10%, the depth of the convection zone decreases by 4%.

Finally we note that the masses we are looking for are lower than the mass 1.497 $M_\odot$ obtained by Eggenberger et al. (2005) in their work. However, we computed a model with the same stellar parameters as these authors and obtained too high a luminosity,

a value of δ_0 about $5\,\mu$Hz or higher, thereby favoring PoMS models. The slope S_0 is positive, but its value is not reliable because it crucially depends on the choice of the mode $\ell = 2$ around $800\,\mu$Hz and around $1142\,\mu$Hz. With Martić et al. (2004) measurements, we obtain a value δ_0 around $4\,\mu$Hz and a negative slope S_0 compatible with MS models.

We have shown that the small spacing $\delta\nu_{01}$ leads to a better criterion for distinguishing MS and PoMS models, since $\delta\nu_{01}$ varies with frequency in opposite way for these two types of models. Moreover, it allows us to estimate the amount of convective-core overshoot for MS models, within the physical assumptions made to compute the models. The observational errors in the quantity $\delta\nu_{01}$ are larger because they are combinations of three frequencies. Indeed, according to the observations of Martić et al. (2004), the estimations of δ_1 and S_1 crucially depend on the point with the highest frequency. The results of the quadratic fit are not reliable. As an example, we obtain a positive slope S_1 and positive curvature γ_1, and these results do not correspond to any model (cf. Fig. 15).

7. Conclusion

Our results show that neither the spectroscopic and interferometric nor the asteroseismic observational constraints are accurate enough to distinguish between main sequence and post-main sequence models of Procyon A. Particularly the dispersion of $2\,\mu$Hz given for the mean large frequency spacing is too high to constrain the models. Moreover, the small frequency spacings $\delta\nu_{02}$ and $\delta\nu_{01}$ give contradictory indications of the age of Procyon A. They are inconsistent with theoretical properties. We have also shown that the detection of frequencies of degrees $\ell = 1$ in the low-frequency range (500 to $800\,\mu$Hz), where mixed modes may appear, are required for determining the evolutionary stage of Procyon.

References

Alecian, G., & Michaud, G. 2005, A&A, 431, 1

Allende Prieto, C., Asplund, M., Garcia Lopez, R. J., & Lambert, D. L. 2002, ApJ, 567, 544

Angulo, C., Arnould, M., Rayet, M., & the NACRE collaboration 1999, Nucl. Phys. A, 656, and WEB site
https://pntpm.ulb.ac.be/Nacre/nacre.html

Bressan, A., Fagotto, F., Bertelli, G., & Chiosi, C. 1993, A&AS, 100, 647

Burgers, J. M. 1969, Flow Equations for Composite Gases (New York Academic Press)

Canuto, V. M., & Mazitelli, I. 1991, ApJ, 370, 295

Chaboyer, B., Demarque, P., & Guenther, D. B. 1999, ApJ, 525, L41

Di Mauro, M. P. 2004, in Helio- and Asteroseismology, Towards a Golden Future SOHO 14 – GONG 2004 Meeting 12–16 Juillet 2004, New Haven USA, ed. D. Danesy, ESA SP-559, 186

Eggenberger, P., Carrier, F., Bouchy, F., & Blecha, A. 2004, A&A, 422, 247

Eggenberger, P., Carrier, F., & Bouchy, F. 2005, New Astron., 10, 195

Garcia, R. A., Lambert, P., Ballot, J., et al. 2006, A&A, sumitted

Gatewood, G., & Han, I. 2006, ApJ, 131, 1015

Girard, T. M., Wu, H., Lee, J. T., et al. 2000, AJ, 119, 2428

Gough, D. O. 1991, Comments on Helioseismic Inference, in Progress of Seismology of the Sun and Stars, ed. Y. Osaki, & H. Shibahashi (Springer Verlag), 283

Guenther, D. B., & Demarque, P. 1993, ApJ, 405, 298

Kervella, P., Thévenin, F., Morel, P., et al. 2004, A&A, 413, 251

Martić, M., & Lebrun, J. C. 2006, A&A, in preparation

Martić, M., Lebrun, J. C., Appourchaux, T., & Korzennik, S. 2004, A&A, 418, 295

Matthews, J., Kushnig, R., Guenther, D. B., et al. 2004, Nature, 430, 51

Mihalas, D., & Weibel-Mihalas, B. 1984, Foundations of Radiation Hydrodynamics (Oxford University Press), 461

Monteiro, M. J. P. F. G., Castro, M., Christensen-Dalsgaard, J., et al. 2005, COROT Week 9, ESTEC, 5–9 December 2005
http://www.astro.up.pt/corot/welcome/meetings/m5/ESTA_CW9_Monteiro_3.pdf

Moreira, O., Appourchaux, T., Berthomieu, G., & Toutain, T. 2005, MNRAS, 357, 191

Morel, P. 1997, A&AS, 124, 597

Morel, P., van't Veer, C., Provost, J., et al. 1994, A&A, 286, 91

Morel, P., Provost, J., Lebreton, Y., Thévenin, F., & Berthomieu, G. 2000, A&A, 363, 675

Morel, P., & Thévenin, F. 2002, A&A, 390, 611

Paquette, C., Pelletier, C., Fontaine, G., & Michaud, G. 1986, ApJS, 61, 177

Perryman, M. A. C., Brown, A. G. A., Lebreton, Y., et al. 1998, A&A, 331, 81

Provencal, J. L., Shipman, H. L., Koester, D., et al. 2002, ApJ, 568, 324

Provost, J., Martić, M., & Berthomieu, G. 2004, in Helio- and Asteroseismology: Towards a Golden Future SOHO 14 – GONG 2004 Meeting 12–16 July 2004, New Haven USA, ed. D. Danesy, ESA SP-559, 594

Provost, J., Berthomieu, G., Bigot, L., & Morel, P. 2005, A&A, 432, 225

Regulo, C., & Roca Cortés, T. 2005, A&A, 444, L5

Schaller, D., Schaerer, D., Meynet, G., & Maeder, A. 1992, A&AS, 96, 269

Steffen, M. 1985, A&AS, 59, 403

Straka, C., Demarque, P., & Guenther, D. B. 2005, ApJ, 629, 1075